Reverse Engineering and Operational Testing of a Machine Element

PETER PANEV*, MIGLENA PANEVA
Institute of Information and Communication Technologies,
Bulgarian Academy of Sciences,
Acad. G. Bonchev str., Block 2, 1113, Sofia,
BULGARIA

**Corresponding Author*

Abstract: - This paper presents an applied reverse-engineering approach for restoring a small damaged polymer component used in a pneumatic distributor. The proposed reconstruction workflow comprises an assessment of the original machine element and its functional requirements, 3D scanning, CAD-based restoration of the damaged region, dimensional evaluation, reproduction by PolyJet additive manufacturing, and verification using manual and software-based measurements. The geometry was acquired using an Artec Micro desktop 3D scanner and processed in Artec Studio 15 Professional. The mating dimensions were verified in relation to the actual machine to confirm installation suitability. The manufactured replacement components exhibited an operational durability comparable to, and in some cases greater than, that of the original part when expressed as the number of manufactured products. Failure occurred in approximately the same region for all specimens. The results confirm the applicability of the 3D scanning-CAD-additive manufacturing workflow for the rapid reconstruction and functional verification of an otherwise unavailable spare part.

Key-Words: - Reverse engineering; Machine element; 3D scanning; Modelling, PolyJet technology; Digital ABS Plus.

Received: March 22, 2026. Revised: July 23, 2026. Accepted: August 18, 2026. Available online: November 18, 2026.

1 Introduction

The maintenance of obsolete or specialized production equipment is frequently hindered by the absence of drawings, the discontinuation of spare-part supply, or the economically inefficient manufacture of a single replacement component. In such cases, reverse engineering enables an existing physical object to be converted into a digital geometric description from which a CAD model can be developed and a replacement part manufactured. [1] demonstrated the recovery of broken and worn machine parts by combining dimensional measurement, geometric reconstruction, and remanufacturing. [2] considered reverse engineering a practical component of maintenance services, particularly when the original design documentation is unavailable. References [3], [4] successfully applied reverse engineering to small-scale components through 3D scanning followed by software-assisted metrological measurements. In addition, rapid prototyping and CAD-model simulation enable the rapid and accurate reproduction of a component for which the design documentation is incomplete. Where the reconstructed geometry proves unsatisfactory, the component can be optimized to improve durability or reduce weight [4], [5].

Optical 3D scanning shortens the geometric-data acquisition stage for components containing free-form surfaces, complex transitions, and areas that are difficult to access. [6] described an integrated procedure in which optical scanning and additive manufacturing were used to reproduce components. An important consideration is that the scanned polygonal mesh does not necessarily constitute the final engineering model. Functional machine components often require the parametric reconstruction of planes, holes, radii, and mating surfaces, together with the engineering restoration of missing regions. The scan therefore serves as a geometric reference, whereas the CAD model provides a controlled manufacturing definition.

The quality of optical measurement depends on the reflective properties of the surface, the component geometry, the viewing angle, and the system settings. Transparent and highly glossy materials are problematic because part of the projected light passes through the object or is reflected specularly. Reference [7] experimentally established that surface coatings affect optical-scanning accuracy and should therefore be applied

uniformly. [8] compared specialized sublimating scanning sprays and showed that coating thickness and sublimation time are important parameters. Thus, a matt coating improves surface visibility but may also introduce a systematic contribution to the measured dimension. For small components in particular, the coating should be as thin and uniform as possible.

In triangulation-based optical systems, surface orientation and visibility affect the completeness of the acquired point data. The conducted work at [9] showed that appropriate positioning of the sensor relative to the measured object increases the reliability of data acquisition.

Additive manufacturing provides a direct transition from a digital model to a physical component and is attractive for small production batches, complex geometries, and rapid functional verification. PolyJet is a suitable technology for the additive manufacture of functional components; it builds the part by depositing photopolymer droplets that are cured layer by layer. The review by [10] demonstrates the increasing use of reverse engineering and additive technologies for spare-part reconstruction. Nevertheless, operational suitability cannot be inferred from geometric conformity alone. Mechanical properties, manufacturing technology, build orientation, local stresses, contact conditions, and the operating environment determine the actual service life. The study by [11] on the friction and wear of additively manufactured polymers emphasizes that contact behavior cannot be assessed solely from nominal material data.

The aim of the present study is to develop and evaluate a practical procedure for restoring a broken transparent polymer distributor element by means of 3D scanning, manual CAD reconstruction, and PolyJet printing. The specific objectives are: (1) to acquire the component geometry after appropriate surface preparation; (2) to reconstruct the missing region in a CAD environment; (3) to verify the mating dimensions; (4) to manufacture three identical replacement parts; and (5) to evaluate their performance under actual operating conditions.

2 Materials and Methods

2.1 Object of Investigation and Operating Conditions

The investigated object is a small machine element located within the aluminum body of a pneumatic distributor. The component is shown in Figure 1. The aluminum body is moved reciprocally to the left and right via an oil-operated pneumatic cylinder.

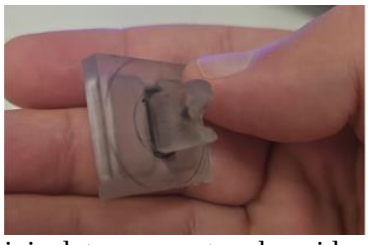


Fig. 1: Original transparent polyamide component showing damage in the region of the protruding mating feature
Source: created by the authors.

The pneumatic distributor operates in a manner similar to a 5/2-type and was specifically designed and manufactured by the possessor of the equipment. The distributor is actuated entirely mechanically and does not employ an electromagnetic solenoid. Figure 2 presents a schematic representation of the distributor and indicates the location of the manufactured component. The detail is presented in two positions of sliding: in left and right and correspond on one cycle.

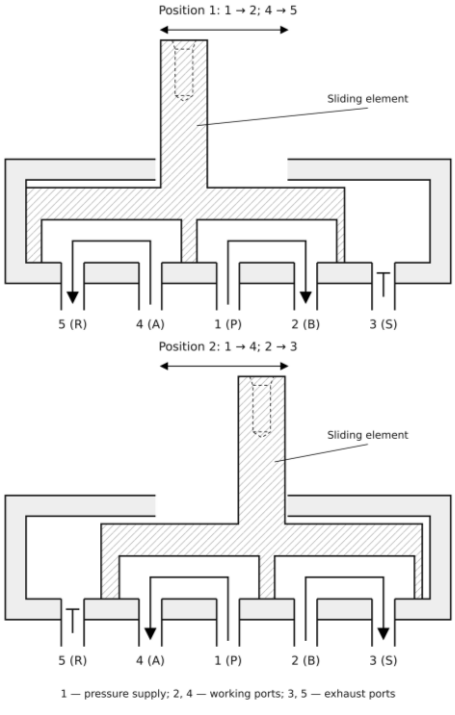


Fig. 2: Pneumatic distributor
Source: created by the authors.

Owing to the lubrication requirements of the pneumatic cylinder, oil droplets are entrained in the compressed-air flow entering the distributor. The operating temperature varies over a relatively wide

range, from +5 °C to +50 °C, while the relative humidity ranges from 40% to 60%. The two profiled recesses on the front face form air-flow channels, while the position of the element provides the distribution function. The operating pressure of the system is approximately 7-8 bar.

The original component was manufactured from an unspecified grade of polyamide by manual milling on a conventional machine tool. Before the present restoration, the component had fractured in the region of the protruding mating feature. Because the exact polyamide grade was unknown, no direct quantitative comparison was made between the mechanical properties of the original material and those of the photopolymer. The original machine element completed approximately 8 000 ÷ 9 000 operating cycles, corresponding to the same number of manufactured products, before failure. The wear and breakage of the component are caused by cyclic mechanical fatigue of the material.

2.2 Preparation for 3D Scanning

The transparency of the original polymer prevented reliable detection of the projected light. Therefore, a thin matt coating of white AESUB scanning spray was applied to the component before scanning. Only the final procedure involving the spray is considered in this paper. The component was scanned using an Artec Micro desktop 3D scanner, designed for small objects and specified by the manufacturer as providing an accuracy of up to 10 μm under appropriate operating conditions [12]. These catalogue specifications should not automatically be interpreted as the accuracy achieved in the present experiment, because the final result depends on surface preparation, calibration, scanning positions, and subsequent data processing. The scanner employs blue light and automated multi-axis object positioning. The component was secured in the Artec Micro holder so that the rotary system provided visibility of the largest possible number of surfaces (Figure 3a).

Scanning was controlled using Artec Studio 15 Professional (Figure 3b). The interface shown in the figure indicates the selected scanning options—High Resolution, Capture Colors, and Move Scans to Origin—as well as a brightness setting of 91%. These values should not be regarded as universally optimal; they were selected for the particular object investigated in this study. To cover the inaccessible regions, two datasets were acquired with the component placed in different orientations and were subsequently aligned.

2.3 Additive Manufacturing

Following reconstruction, the machine element was reproduced using a Stratasys Objet260 system [13].



a) b)

Fig. 3: Preparation for scanning: a) component mounted in the Artec Micro holder; b) Artec Studio 15 Professional scanning interface.
Source: created by the authors.

Based on an assessment of the materials compatible with this technology, Digital ABS Plus photopolymer was selected as the most suitable material for manufacturing the machine elements [14], [15]. According to the manufacturer, Digital ABS Plus was developed for functional prototypes requiring greater strength and temperature resistance than standard rigid photopolymers [14]. Digital ABS Plus is a two-component material, consisting of the material RGD 515S, which is the basis and RGD 531 - a strengthening component. The mechanical properties of the material have been validated by the authors in previous publications, with the majority of the values corresponding to those specified in the technical specifications. The parameters are presented in Table 1.

Table 1. Mechanical properties of material Digital ABS Plus, obtained by the authors

Parameters	**Value**
Tensile strength, Rm	54÷57 MPa
Modul of elasticity, E	2.25 GPa
Elongation, *e*	5%
Roughness on the top, Ra	2.23 μm
Roughness perpendicular of the layers, Ra	3.18 μm
Hardness, Shore D	83,4
Impact strength, Charpy test	10.82 kJ/m^2

Source: created by the authors.

The direction of printing of the element is carried out along the X-Y axis, and the height is built along

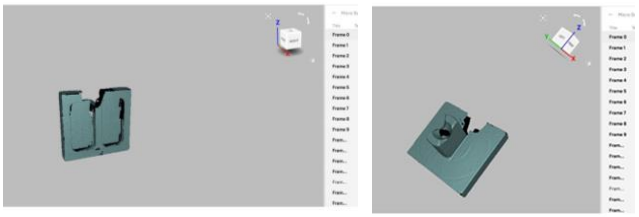
the Z axis. The printing parameters comprised a layer thickness of 30 μm, a matt surface finish, and SUP705B support material [16], [17]. The support material was used for overhanging and internal regions, and the component was fully surrounded to promote uniform build conditions. After printing, the support material was removed using a high-pressure WaterJet system for about 5 min. The system is manufactured by the material producer, Stratasys. It operates in conjunction with a maximum pressure of 110-bar water jet. and the component was allowed to dry on a level surface for at least 24 h.

3 Results

3.1 Digital and Physical Reconstruction

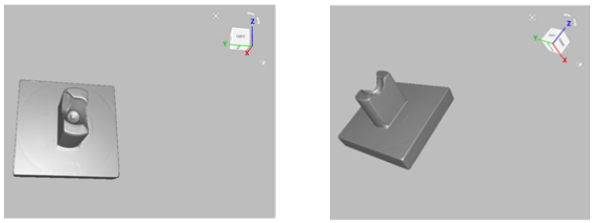
3.1.1 3D Scanning and Scan Processing

Surface preparation was performed by applying a thin layer of matt scanning spray, which enabled the transparent original component to be captured and complementary scans to be obtained. The component was scanned in two orientations, as shown in Figure 4a and Figure 4b, and the datasets were processed in Artec Studio 15 Professional. The two scans were inspected and manually aligned using the Align command and corresponding geometric regions. Following alignment, the data were merged using Sharp Fusion. The Fix Holes operation was also applied where required to close residual openings and obtain a complete mesh. The resulting polygonal geometry clearly reproduced the base plate, the two front air channels, and the remaining portion of the rear protrusion. The merged model is shown in Figure 5. The scan also retained features associated with the actual condition of the component, including the fracture and local surface irregularities.



a) b)

Fig. 4: Partial scans acquired from different orientations before final merging: a) rear view; b) view of the front air channels.
Source: created by the authors.



a) b)

Fig. 5: Merged geometry after alignment and Sharp Fusion: a) front-side view; b) right: rear-side view.
Directly printing the scanned geometry would therefore have reproduced the defect; parametric reconstruction was required to restore the nominal form.
Source: created by the authors.

3.1.2 CAD Reconstruction and Verification

Figure 6 presents the final merged triangulated model used as the geometric reference for reconstruction. The triangulated model served as both a visual and geometric reference in the CAD environment. The CAD model was created parametrically rather than by directly converting the polygonal mesh into a solid body.

The principal dimensions were determined and compared using three sources: available dimensional information, the scanned geometry, and manual calliper measurements of the original component. The region missing as a result of the fracture was reconstructed by restoring the original form; the hole in this region was identified as a Ø2.4 mm threaded hole. This compromised area therefore required geometric reconstruction. No deliberate increase in thickness or transition radius was introduced in the critical region. Views of the reconstructed CAD model are presented in Figure 7. The principal dimensions were measured in the software, and the scan data were compared with the calliper measurements. This procedure ensured compatibility at the main mating interfaces.

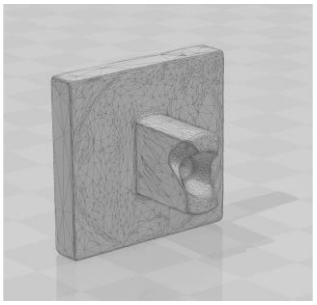
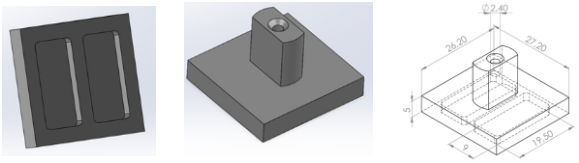


Fig. 6: Final merged triangulated 3D model used as a reference for CAD reconstruction.
Source: created by the authors.

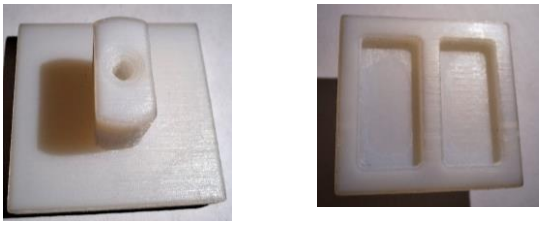


a) b) c)

Fig. 7: Reconstructed parametric CAD model: a) front face with two air channels; b) rear face with the protruding mating feature and hole; c) dimensions evaluated in the CAD environment.
Source: Source: created by the authors.

3.1.3 Additive Manufacturing and Dimensional Verification

Three identical components were manufactured from Digital ABS Plus on a Stratasys Objet260 system using PolyJet technology. The printing time for one component was 1 h 12 min. After printing, the support material was removed using high-pressure water; no additional mechanical or thermal post-processing was applied. The finished 3D-printed component is shown in two views in Figure 8. Additive manufacturing was selected because it enables the rapid production of a small batch and permits direct comparison between the operational performance of the printed replacement and that of the conventionally milled polymer component. The initial digital preparation required approximately 2-3 h. Furthermore, the high accuracy of the 3D scanner provided a reliable geometric basis for reconstruction and limited the likelihood of substantial modelling deviations. Once the final model had been created, repeated production required neither rescanning nor additional modelling.



a) b)

Fig. 8: Finished Digital ABS Plus component: a) rear face with the protruding mating feature; b) front face with the air channels.
Source: created by the authors.

Verification of the reconstructed machine element was conducted in two consecutive stages. First, the reconstructed scan-based model was compared with the geometry of the 3D-printed machine element. The principal mating dimensions of all three printed components were measured using a caliper with a stated resolution of 0.1 mm, and the values were averaged. Mean values are reported to 0.01 mm solely for calculation purposes. The component was also rescanned, and its principal geometric parameters were measured using the point-to-point measurement function in Artec Studio 15 Professional (Figure 9). Before the measurements were performed, the polygonal model was oriented relative to the global Cartesian coordinate system so that its principal surfaces were approximately parallel to the XY, XZ, and YZ coordinate planes. This orientation facilitated the reproducible selection of the characteristic points defining each investigated dimension.

For each measurement, two geometrically corresponding points were selected interactively on the polygonal surface. Depending on the dimension being evaluated, these points were located on opposite external edges, parallel surfaces, channel boundaries, hole contours, or the extremities of the protruding mating feature. The software assigned Cartesian coordinates $P_1(x_1, y_1, z_1)$ and $P_2(x_2, y_2, z_2)$ to the selected positions relative to the active model coordinate system.

The coordinate differences were calculated as follows:

$$\Delta x = x_2 - x_1, \quad \Delta y = y_2 - y_1, \quad \Delta z = z_2 - z_1 \tag{1}$$

The direct point-to-point distance was then determined by Artec Studio according to the Euclidean relationship:

$$L = \sqrt{((\Delta x)^2 + (\Delta y)^2 + (\Delta z)^2)} \tag{2}$$

For dimensions corresponding to a specific principal direction of the component, the relevant absolute coordinate difference—|Δx|, |Δy|, or |Δz|—was used. The full three-dimensional point-to-point distance L was used when the selected points did not lie along a single coordinate axis. To reduce errors associated with the manual selection of points, the model was displayed in an appropriate orthographic view and enlarged before each measurement. The selected points were placed on clearly identifiable geometric features corresponding to those used for the calliper measurements and in the CAD model.

All measurement data are presented in Table 2 (Appendix). This procedure verified the conformity of the principal surfaces, contours, holes, and mating regions.

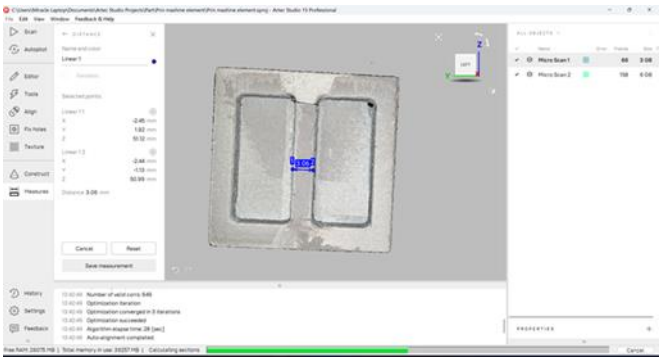


Fig. 9: Metrological verification of geometric accuracy using Artec Studio 15 Professional.
Source: Source: created by the authors.

Dimensional deviations and relative errors were calculated using the following numerical relationships:

$$\Delta_i = X_i - X_{CAD,i} \quad (3)$$

$$\delta_i = \frac{|\Delta_i|}{X_{CAD,i}} \cdot 100\% \quad (4)$$

where Δ_i is the signed deviation and δ_i is the absolute relative error. Table 3 summarizes the arithmetic deviation measures obtained from the caliper and 3D-scanning measurements.

The caliper measurements yielded a mean absolute deviation of 0.046 mm, a root-mean-square deviation of 0.056 mm, and a mean absolute relative error of 0.919%. The maximum absolute deviation was 0.13 mm and occurred in the distance between the two air channels. These differences should be interpreted with reference to the stated caliper resolution of 0.1 mm.

For the 3D-scanning measurements, the mean absolute deviation from the CAD model was 0.061 mm, the root-mean-square deviation was 0.080 mm, and the mean absolute relative error was 0.800%. The maximum absolute deviation was 0.20 mm and corresponded to the overall height of the component.

The mean signed deviations were -0.024 mm for the caliper measurements and -0.036 mm for the 3D-scanning measurements.

The mean paired difference between the absolute deviations obtained by 3D scanning and calliper measurement was 0.015 mm. The positive value indicates slightly greater absolute deviations for the 3D-scanning method; however, the difference was not statistically significant, confirmed by the paired-samples T-test: (t(11)=0.804), (p=0.438), with a 95% confidence interval from −0.026 to +0.056 mm.

Table 3. Summary statistics of the geometric deviations.

Parameter	Calliper measurement	3D-scanning measurement
Mean signed deviation	-0.024 mm	-0.036 mm
Mean absolute deviation	0.046 mm	0.061 mm
Root-mean-square deviation (RMS)	0.056 mm	0.080 mm
Mean absolute relative error	0.919%	0.800%
Maximum absolute deviation	0.13 mm	0.20 mm

Source: created by the authors.

The second stage of geometric verification consisted of a physical fit and operational check. The component could be installed in the aluminum body and successfully perform its distribution function. The metrological results, together with the successful installation and operation of the printed components in the machine, confirm the geometric and functional conformity of the reconstructed model.

3.2 Operational Results

Each manufactured component was installed in the actual machine and operated until a failure occurred that prevented further machine operation. One operating cycle corresponded to one manufactured product. The reported values were obtained from approximate production counters, and all components were subjected to comparable operating conditions. Nevertheless, the procedure did not constitute a standardized laboratory test under strictly controlled loading conditions. Table 4 presents the service-life results for the three printed components. The data are compared with the durability of the original polyamide machine element. The cycle count values for each of the polymer details are based on the number of components produced by the machine, as recorded by counters.

All three components fractured in approximately the same region, namely around the protruding mating feature. After this region fractured, the machine could no longer operate. The repeatability of the failure location is an important qualitative result because it directs attention towards the local geometry and loading conditions rather than towards a random failure in an arbitrary region.

Table 4. Results of the operational evaluation of the three printed components

Component	Material	Appr. cycles	Observation
1	Digital ABS Plus / PolyJet	9 000	Failure in the critical region
2	Digital ABS Plus / PolyJet	15000	Failure in approximately the same region
3	Digital ABS Plus / PolyJet	11500	Failure in approximately the same region

Source: created by the authors

4 Discussion

The results indicate good agreement between the CAD model and the machine elements manufactured using PolyJet technology. The mean absolute deviations for both measurement methods were below 0.1 mm. The root-mean-square deviations also remained low, at 0.056 and 0.080 mm, respectively. These findings confirm that the applied sequence of 3D scanning, parametric reconstruction, and additive manufacturing can reproduce the principal geometric and mating characteristics of the damaged machine element.

Minor differences were observed between the two measurement methods. The caliper measurements produced lower mean absolute and root-mean-square deviations, whereas the mean absolute relative error obtained by 3D scanning was slightly lower. This difference can be attributed to the distinct measurement principles. A caliper determines individual linear dimensions between selected contact points, whereas 3D scanning represents the entire surface, and its results depend on alignment, the selection of measurement sections, triangulation, and polygonal-mesh processing. The applied matt spray, the geometric complexity of the channels, and the removal of the support material may also have influenced the results.

The largest signed deviation in the caliper measurements was -0.13 mm and occurred for the distance between the channels. For 3D scanning, the largest difference was -0.20 mm and corresponded to the overall height of the component. Nevertheless, successful installation in the aluminum body and normal execution of the distribution function demonstrate that the measured deviations did not compromise functional compatibility.

From a physical perspective, the slight reduction in dimensions may result from volumetric shrinkage during photopolymerization, subsequent post-curing and material stabilization, or the development of residual stresses during the layer-by-layer build process. The magnitude and direction of these changes can depend on the print orientation, local cross-sectional thickness, the amount of support material, and the constraint of deformations by adjacent regions.

A negative mean signed deviation should not be interpreted as evidence of uniform isotropic shrinkage. Table 2 (Appendix) shows both negative and positive individual deviations. Consequently, while the values indicate a slight overall tendency toward smaller dimensions, they do not demonstrate uniform shrinkage of the entire part. The low mean signed deviations do not indicate a substantial systematic dimensional error.

The geometric results were further supported by the operational evaluation. The original polyamide component completed approximately 8 000-9 000 cycles, whereas the three Digital ABS Plus components achieved approximately 9 000, 15 000, and 11 500 cycles. The estimated mean service life of the printed components was approximately 11830 cycles. The additively manufactured replacements therefore exhibited a service life comparable to or greater than that of the original component.

The recurrence of fracture in approximately the same region suggests that the cause was probably related to the local geometry and stress concentration around the protruding mating feature. This hypothesis cannot be confirmed conclusively without stress analysis and examination of the fracture surfaces. Future work should therefore investigate an increased transition radius, local reinforcement of the cross-section, and a comparison between the original and an optimized design.

5 Future Steps

Future steps involve subjecting the manufactured machine components to tomographic analysis to verify their internal homogeneity and comparing the data with that of conventionally manufactured parts. Another important study involves analyzing the material's wear resistance across various print orientations, conditions, and loads. This approach will enable a detailed analysis of the material and its suitability for the production of spare parts.

6 Conclusion

The developed workflow, comprising 3D scanning, parametric reconstruction of the geometry, PolyJet manufacturing, and metrological analysis through manual and software-based verification, enabled the successful restoration of the damaged polymer machine element.

Quantitative verification yielded a mean absolute deviation of 0.046 mm for the caliper measurements and 0.061 mm for the 3D-scanning measurements. The corresponding mean absolute relative errors were 0.919% and 0.800%, demonstrating good agreement between the CAD model and the manufactured component.

Despite the observed local differences, the components were successfully installed and performed the intended distribution function at an operating pressure of approximately 7-8 bar. The service life of the reconstructed machine elements was comparable to or greater than the number of cycles recorded for the original polyamide component.

The results confirm the applicability of 3D scanning and additive manufacturing for restoring small spare parts when complete design documentation is unavailable. Further geometric optimization of the failure region and controlled testing using a larger number of specimens are required to increase operational durability and establish the statistical reliability of the observed performance.

Declaration of Generative AI and AI-assisted Technologies in the Writing Process

During the preparation of this work, the author(s) utilized artificial intelligence (AI) technologies solely for the purpose of linguistic refinement and grammatical correction. Following the application of these tools, the author(s) comprehensively reviewed, verified, and edited the resulting text. The author(s) maintain full accountability and responsibility for the accuracy, integrity, and final content of the publication.

References:

[1] Bagci, E., Reverse engineering applications for recovery of broken or worn parts and re-manufacturing: Three case studies. *Advances in Engineering Software*, 40 (2009), 407–418. https://doi.org/10.1016/j.advengsoft.2008.07.003.

[2] Dúbravčík, M.; Kender, Š., Application of Reverse Engineering Techniques in Mechanics System Services, *Procedia Engineering*, 48 (2012), 96–104. https://doi.org/10.1016/j.proeng.2012.09.491.

[3] Todorov T., Bankov B., Zagorski M., Gavrilov T. and Dimitrov K., Rapid Prototyping and Measuring Assessment of a Complex Geometry, *XXXIV International Scientific Symposium Metrology and Metrology Assurance (MMA)*, Sozopol, Bulgaria, 2024, pp. 1-4, https://doi.org/10.1109/MMA62616.2024.10817673.

[4] Zagorski M, Miltchev R., Nikolov N., Ivanov T., Reverse engineering and optimization of small-scale objects for humanoid robotic systems. *AIP Conf. Proc.*, 3 March 2025; 3274 (1): 050013. https://doi.org/10.1063/5.0258475.

[5] Nawawithan N., Kittisakpairach P., Nithiboonyapun S., Ruangjirakit K., Jongpradist P., Lightweight bumper design for crash safety and pedestrian protection. *AIP Conf. Proc.*, 17 May 2024; 3086 (1): 030003, https://doi.org/10.1063/5.0204999.

[6] Paulic, M.; Irgolic, T.; Balic, J.; Cus, F.; Cupar, A.; Brajlih, T.; Drstvensek, I. Reverse Engineering of Parts with Optical Scanning and Additive Manufacturing, *Procedia Engineering*, 69 (2014), 795–803. https://doi.org/10.1016/j.proeng.2014.03.056.

[7] Pereira, J. R. M.; Penz, I. de L. e S.; da Silva, F. P., Effects of different coating materials on three-dimensional optical scanning accuracy, *Advances in Mechanical Engineering*, 11(4) (2019), 1–6. https://doi.org/10.1177/1687814019842416.

[8] Franke, J.; Koutecký, T.; Koutný, D., Comparison of Sublimation 3D Scanning Sprays in Terms of Their Effect on the Resulting 3D Scan, Thickness, and Sublimation Time. *Materials*, 16(18) (2023), 6165. https://doi.org/10.3390/ma16186165.

[9] Heczko, D.; Oščádal, P.; Kot, T.; Huczala, D.; Semjon, J.; Bobovský, Z., Increasing the Reliability of Data Collection of Laser Line Triangulation Sensor by Proper Placement of the Sensor, *Sensors*, 21(8) (2021), 2890. https://doi.org/10.3390/s21082890.

[10] Dalpadulo, E.; Petruccioli, A.; Gherardini, F.; Leali, F., A Review of Automotive Spare-Part Reconstruction Based on Additive Manufacturing, *Journal of Manufacturing and Materials Processing*, 6(6) (2022), 133. https://doi.org/10.3390/jmmp6060133.

[11] Dangnan, F.; Espejo, C.; Liskiewicz, T.; Gester, M.; Neville, A., Friction and wear of additive manufactured polymers in dry contact,

Journal of Manufacturing Processes, 59 (2020), 238–247. https://doi.org/10.1016/j.jmapro.2020.09.051.

[12] Artec 3D, Artec Micro: desktop 3D scanner for small objects (manufacturer information), 2019, [Online] https://www.artec3d.com/news/artec-micro-release (Accessed Date: January 20, 2026).

[13] Stratasys, Objet260 Connex1/2/3—system specifications and supported materials, [Online]. https://support.stratasys.com/en/Printers/PolyJet-Legacy/Objet260-Connex-1-2-3 (Accessed Date: January 20, 2026).

[14] Stratasys, Digital ABS Plus—PolyJet material data sheet, 2024, [Online]. https://www.stratasys.com/siteassets/materials/materials-catalog/polyjet-materials/digital-abs-plus/mds_pj_digitalabsplus_a4_0524a-1.pdf (Accessed Date: January 20, 2026).

[15] Yahamed, A., Joyce, M., Fleming, P. D., Pekarovicova, A., & Ikonomov, D. P., Polymers for 3D Printed Structures, Precision, Topography and Roughness. *RA Journal of Applied Research*, 2018, 4(12), 2160–2169. https://doi.org/10.31142/rajar/v4i12.04.

[16] Stratasys, PolyJet Support Materials: SUP705/SUP705B, [Online]. https://support.stratasys.com/en/Materials/PolyJet/PolyJet-Support (Accessed Date: January 20, 2026).

[17] Standard ISO/ASTM 52900:2021. Additive manufacturing — General principles — Fundamentals and vocabulary. International Organization for Standardization, 2021, [Online]. https://www.iso.org/standard/74514.html (Accessed Date: January 15, 2026).

Contribution of Individual Authors to the Creation of a Scientific Article (Ghostwriting Policy)

- Miglena Paneva carried out the research and the methodology of the process.
- Peter Panev executed the 3D scanning of the machine element.
- Peter Panev and Miglena Paneva made reproduction of CAD models and analyzed the data.

Sources of Funding for Research Presented in a Scientific Article or Scientific Article Itself

The research was carried out as part of project No. KP-06-M87/4 “Research the wear resistance of machine elements, possibilities for optimizing their properties through innovative methods and materials”, financed by the Bulgarian National Science Fund.

Conflict of Interest

The authors have no conflicts of interest to declare that are relevant to the content of this article.

Creative Commons Attribution License 4.0 (Attribution 4.0 International, CC BY 4.0)

This article is published under the terms of the Creative Commons Attribution License 4.0 https://creativecommons.org/licenses/by/4.0/deed.en

APPENDIX

Table 2. Verification measurements obtained using a calliper and 3D scanning.

Geometric parameter	CAD model, mm	Calliper measurements			Measurements obtained by 3D scanning		
		Mean measured value, mm	Deviation, mm	Relative error, %	Measured value, mm	Deviation, mm	Relative error, %
Overall length of the base plate	26.2	26.23	0.03	0.11	26.16	-0.04	0.15
Overall width of the base plate	27.2	27.17	-0.03	0.11	27.17	-0.03	0.11
Base-plate thickness	5	4.93	-0.07	1.40	5.06	0.06	1.20
Overall component height	17	16.97	-0.03	0.18	16.8	-0.20	1.18
Length of the protruding mating feature	6	6	0	0.00	5.9	-0.10	1.67
Width of the protruding mating feature	5.8	5.73	-0.07	1.21	5.76	-0.04	0.69
Height of the protruding mating feature	12	11.97	-0.03	0.25	11.94	-0.06	0.50
Hole diameter	2.4	2.37	-0.03	1.25	2.41	0.01	0.42
Air-channel length	19.5	19.53	0.03	0.15	19.51	0.01	0.05
Air-channel width	9	9.07	0.07	0.78	8.89	-0.11	1.22
Air-channel depth	2.4	2.37	-0.03	1.25	2.41	0.01	0.42
Distance between the channels	3	2.87	-0.13	4.33	3.06	0.06	2.00

Source: created by the authors.